Microwave-Assisted Synthesis of Core–Shell Nanoparticles—Insights into the Growth of Different Geometries

Aisha A. Womiloju, Christiane Höppener,* Ulrich S. Schubert, and Stephanie Hoeppener*

Microwave irradiation is utilized for the rapid synthesis of gold–silver core–shell bimetallic nanoparticles (NPs) in a two-step process. A strategy of establishing a bilayer organic barrier around the core using citrate and ascorbic acid as capping agents, providing a means to achieve a well-defined boundary layer between the core and the shell material, is reported. These boundary layers are essential for synthesizing different core–shell morphologies and the approach results in tunable bimetallic NPs with defined core–shell structures, both for spherical as well as for triangular seed cores. In addition, theoretical calculations of the plasmonic characteristics based on the boundary element method of different classes of NPs are conducted. These investigations enable conclusions to be drawn on the influence of the core morphology on the tunability of their localized surface plasmon resonances.

1. Introduction

Bimetallic core–shell nanoparticles (NPs) have generated increasing research attention in recent years. These hybrid NPs provide the synergetic effect of the individual constituent metals, originating from plasmonic coupling effects, which

A. A. Womiloju, Prof. U. S. Schubert, Dr. S. Hoeppener
Laboratory for Organic and Macromolecular Chemistry (IOMC)
Friedrich Schiller University Jena
Humboldtstr. 10, Jena 07743, Germany
E-mail: s.hoeppener@uni-jena.de
A. A. Womiloju, Prof. U. S. Schubert, Dr. S. Hoeppener
Jena Center for Soft Matter (JCSM)
Friedrich Schiller University Jena
Philosophenweg 7, Jena 07743, Germany
Dr. C. Höppener
Leibniz-Institute of Photonic Technology (IPHT)
Albert-Einstein-Straße 9, Jena 07745, Germany
E-mail: christiane.hoeppener@leibniz-ipht.de
Dr. C. Höppener
Institute for Physical Chemistry
Friedrich Schiller University Jena
Lessingstraße 10, Jena 07743, Germany

help to access a variety of different attractive properties of core–shell NPs. These include, e.g., an increased enhancement factor for sensing applications or to establish efficient catalytic properties.[1–4] For instance, literature data has shown that gold NPs are easily tailored in terms of homogeneity and biocompatibility,[5–7] however they provide, e.g., no antimicrobial activity. In comparison, silver NPs provide higher extinction coefficients,[6] catalytic properties and antimicrobial activity, but these properties are associated with a rather high cytotoxicity.[5] Core–shell bimetallic plasmonic NPs consisting of gold NPs as core material and silver as shell (Au@Ag) have been widely reported in literature due to the unique properties exhibited when the core or the shell is rationally tuned.[8,9] Au@Ag NPs with Ag-like optical properties show, at the same total metal ion concentrations, a lower effective silver concentration compared to AgNPs of the same size. As a consequence, Au@Ag NPs have, e.g., been reported to show a negligible toxicity to human dermal fibroblasts.[4] Furthermore, due to their large enhancement factor and strong antibacterial activity, Ding et al. could demonstrate the use of Au@Ag core–shell NPs for two photon imaging of bacteria utilizing near infra-red femtosecond laser pulses.[7] A shell thickness dependent antibacterial activity was reported by Yang et al.[10] Sensor properties of core–shell NPs for surface enhanced Raman spectroscopy (SERS) applications have also been explored.[3,11]

Frequently, studies on metal NP synthesis rely on thermal, electrochemical, sonochemical and photochemical reduction techniques.[12,13] However, the extremely short reaction times of microwave synthesis, when combined with well-established synthesis routes, such as, coprecipitation, have been proven to be highly suitable for the synthesis of colloidal NPs.[14] This approach has been reported to be tremendously efficient in the improvement of the particle quality by reducing undesired side reactions, increased product yield, improved reproducibility, and excellent control of reaction parameters.[13,15] Moreover, a significant improvement can be achieved in terms of avoiding the use of organic solvents and hazardous chemicals. Motivated by these advantages, also bimetallic hybrid NPs have been synthesized by microwave-assisted processes. Tsuji et al. reported a microwave-polyol approach for the synthesis of core–shell Au@Ag NPs with an ethylene glycol polymer capping.[16] Au and Ag provide almost identical face centered cubic (fcc) crystal structures and lattice constants. As a consequence, synthesizing

them in a core–shell NP imposes a number of challenges.[17] A major problem associated with the synthesis of bimetallic core–shell NPs is the preferential formation of alloy composites, resulting in an indistinctive core–shell layer boundary.[8] Phase images from high resolution transmission electron microscopy (HRTEM) images are often required to distinguish the crystal facets. As a consequence, the selective tuning of the core and (or) the shell to tailor the localized surface plasmon resonance (LSPR) becomes difficult. Here, we utilize microwave synthesis by adopting the commonly used Turkevich method for core NP syntheses to obtain well-defined gold NPs.[13,18,19] A strategy for the formation of a silver shell around the gold core with well-defined layer boundaries, which can be selectively tuned, was established by the use of citrate and ascorbic acid (A/A) as capping agents. This approach creates a robust organic barrier layer on the gold NP surface, which preserves the gold core structure during the subsequent silver attachment. We also directed our efforts toward the synthesis of gold nanoprisms as core materials and utilized bis-(p-sulfonatophenyl) phenylphosphine dihydrate dipotassium (BSPP) as barrier layer. This barrier layer facilitates a subsequent use of these gold nanoprisms as seeds for the silver shell formation. All synthesized core–shell NP architectures were characterized regarding their morphological, optical, structural and elemental composition. Moreover, simulation of the plasmonic properties of different NP architectures were conducted by means of boundary element (BEM) calculations.

2. Spherical Core–Shell NP Architectures

In a first optimization step, uniform spherical gold NP serving as core material were synthesized by improving the microwave heating approach via optimizing the microwave operational modes (see Section S1 in the Supporting Information for detailed information on the optimization of microwave operational modes). Typically, the synthesis routes for plasmonic particles involve reduction, nucleation, growth and reshaping processes. At the same time, the total microwave irradiation time can be divided into a ramp time (time span required to reach the desired reaction temperature) and the retention time (time span of constant temperature during irradiation). The reduction and nucleation of the metal salt is

expected to take place within the ramp time, while NP growth and reshaping take place during the retention time.[13,20] Two heating approaches can be tested with the Biotage single mode microwave system, namely the constant power mode (which efficiently controls the ramp time and ensures fast reduction of the metal salt) and the constant temperature operational mode (which manages the retention time which, in turn, controls NPs growth and reshaping processes). The influence of both modes on the NP synthesis is elaborated in the Supporting Information (Section S1, Supporting Information).

The reactions to optimize the NP production were performed by separately synthesizing AuNPs from combinations of $HAuCl_4$/ethanol (seed 1), $HAuCl_4$/ethanol/citrate (seed 2) and $HAuCl_4$/ethanol/citrate/ascorbic acid (A/A) (seed 3).

Spherical gold NPs with a narrow size distribution and an average particle size of 15 ± 2 nm were obtained for seed 2 (**Figure 1**a) and seed 3. The size of the as-synthesized NPs remained unchanged, utilizing only citrate (seed 2) or citrate combined with ascorbic acid (seed 3) as capping agents. The UV–vis spectra revealed no significant change in the LSPR band (λ_{max}), which is ascribed to the maximum at 524 nm in both cases (Figure 1b). A stronger absorption was however observed for the ascorbic acid stabilized AuNPs. The main reason for this behavior is that ascorbic acid contributes to the reduction of the gold salt and results in an increase of the population of the gold NPs. At the same time, the ascorbic acid is supposedly not contributing to the particle growth, as evidenced by the unchanged size of the obtained NP seeds. However, it forms a capping layer around the gold NPs, thereby providing an organic barrier around the NPs. This leads to the synthesis of highly stable solutions of Au NPs. A higher absorption was also observed for the Au seeds synthesized without citrate and ascorbic acid, which show a red shift in the absorption maximum located at λ_{max} at 560 nm (Figure 1b). This is indicative for the presence of highly reactive unoccupied surface sites, which provide potential adsorption sites for NP growth and aggregation according to the nucleation and growth processes described by the LaMer model.[21,22] The broadening of the LSPR band is moreover indicative for an inhomogeneous particle size distribution and aggregation.

In the next step, Au@Ag core–shell NPs were synthesized from citrate stabilized (seed 2) and citrate/ascorbic acid stabilized Au cores (seed 3). For this purpose, the respective
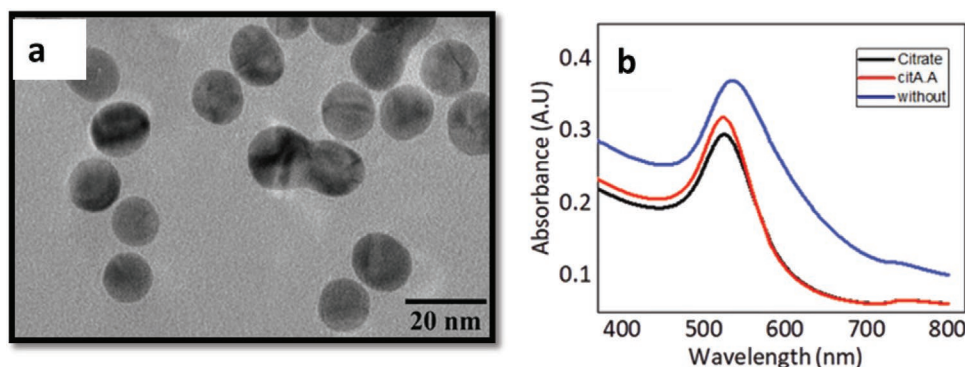

Figure 1. a) TEM image of rather monodisperse citrate-ascorbic acid stabilized gold NP synthesized at a microwave power of 100 W for 60 s. b) UV–vis spectrum of spherical Au NPs (Blue: Without capping agent, Red: Citrate-ascorbic acid capping. Black: Only citrate capping).
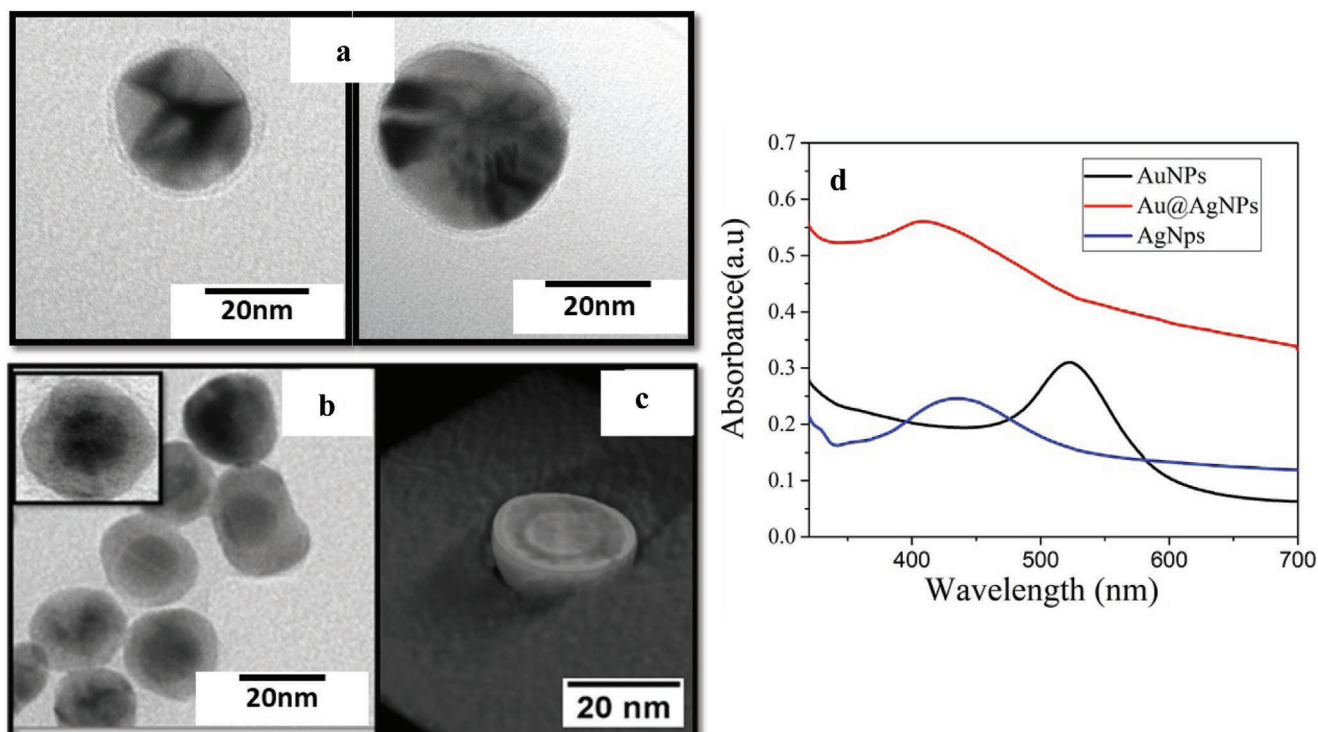
ADVANCED
SCIENCE NEWS
www.advancedsciencenews.com

Particle
& Particle Systems Characterization
www.particle-journal.com

Figure 2. TEM images of a) bimetallic alloy composite and b) Au@Ag core–shell bimetallic NPs (Inset: Detailed view on the well-defined core–shell layer boundary). The silver shell formation was established with 300 W and 60 s microwave irradiation time. c) TEM tomography reconstruction showing the core–shell structure (contrast of core and shell are inverted for better visualization). The corresponding bright-field TEM image can be found in the Supporting Information (Figure S4, Supporting Information). d) UV–vis spectrum of Au, Ag, and Au@Ag NPs.

aqueous solutions of silver acetate, citrate and ascorbic acid were comixed.

The Ag shell formation was observed at a MW power of 300 W and an irradiation time of 60 s. The formation of alloy gold-silver composite NPs without defined core–shell boundaries was observed when utilizing gold seed 2 with only a citrate capping (**Figure 2**a).

HR-TEM investigations (Figure S5, Supporting Information) on individual core–shell NPs suggest that the Ag shell formed around the polycrystalline Au core is also polycrystalline, indicating a nonepitaxial growth of the shell around the respective cores.

The core–shell NP formation is attributed to the fact that the kinetic stabilization from the available citrate ion on the Au surface at elevated temperatures is insufficient or too weak to provide a well-defined organic barrier layer.[22,23] When using the citrate-ascorbic acid stabilized Au NPs as core material (seed 3), Ag shell formation was observed at a higher power of 300 W and 60 s irradiation time compared to the 100 W power, which was required for the synthesis of the Au core. This implies that the reduction of the silver salt requires more demanding conditions compared to the reduction of the gold salt performed in a MW reaction.

The corresponding TEM images depicted in Figure 2b confirmed the reduction of the silver salt on the gold core (Au@Ag) surface rather than forming new nucleation sites, as seen from the distinct boundaries of the NP core and shell. In this case, the addition of ascorbic acid with citrate on the gold seeds seems to provide a higher thermal stability and, thus,

prevents the depletion of the capping by high temperature and, hence, provides an organic surface barrier for the silver attachment.

TEM tomography was used to further characterize the core–shell NPs. The images were collected at a tilt range of +60° to − 60° with an increment of 2°. A cross-sectional cut of the reconstructed tomogram approximately at the center of the NP is shown in Figure 2c. Furthermore, the elemental composition of the spherical Au@Ag NP was examined utilizing energy dispersive X-ray spectroscopy (EDX) and HAADF STEM investigations and the result is depicted in **Figure 3** and Figure S6 (Supporting Information) confirming the presence of Au as well as of Ag.

The EDX measurement (Figure 3) does not provide a sufficiently high resolution for mapping and resolving the individual metal layers, however, characteristic peaks originating from Au and Ag, which confirm the presence of both metals within the particle could be obtained. Additional Cu peaks originate from the TEM grid itself and are found also in areas, which do not include particles. These results led to the conclusion that the gold-silver bimetallic NPs synthesized by microwave irradiation are composed of a dense gold core and are surrounded by a silver shell.

The UV–vis absorbance spectrum of the Au@Ag NPs (Figure 2d) shows a unique spectrum, which is mostly dominated by the silver shell. The core–shell NPs revealed a λ_{max} at 409 nm. This can be attributed to the thickness of the shell ($d > 5$ nm) which results in silver-like optical properties of the NPs.[1] The high absorbance of the Au@Ag NPs and the broad
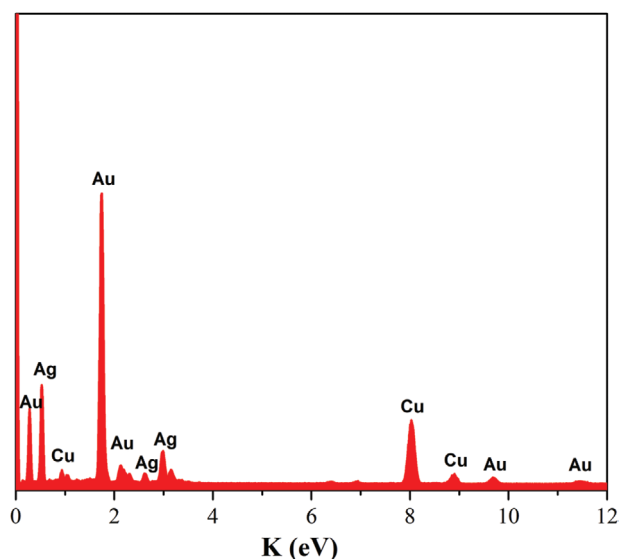
**ADVANCED
SCIENCE NEWS**
www.advancedsciencenews.com

Particle
& Particle Systems Characterization
www.particle-journal.com

Figure 3. EDX measurement revealing the presence of the characteristic Au and Ag peaks.

Figure 4. Comparison of FT-IR spectra of citrate-ascorbic acid capped Au NPs (red) used as core and citrate capped Au@Ag NPs (blue).

peak shape suggest a high population of particles with a relatively large size distribution. In addition, influences due to Ostwald ripening on the morphology of the silver shell were observed, which is reflected by the non-uniform Gaussian-like appearance of the spectrum.[18] For comparison, the synthesis of single metallic silver NPs was carried out in the power controlled reaction mode using the same amount of precursor as used for the synthesis of the silver shell. The Ag NPs synthesis was achieved in 60 s irradiation time at a power of 300 W. Silver NPs with an average size of 50 nm were synthesized (Figure S7, Supporting Information). The UV–vis spectra of the particles displayed a broad band with a λ_{max} at 436 nm as shown Figure 2d. The synthesis time and irradiation power for the AgNP synthesis were observed to be the same as required to establish the silver shell deposition during the Au@Ag NPs synthesis. Below this time and at a lower microwave power, the silver salt was not reduced, thus, no NP synthesis was observed. The longer synthesis time required for the reduction of silver acetate by ascorbic acid is reasonable due to the absence of high microwave absorbing reagents such as ethanol. A measure of the microwave absorptivity of a solvent known as the loss tangent (tan∂) ranges from tan $\partial > 0.5$, tan ∂ 0.1 – 0.5 and tan $\partial < 0.1$ for highly absorbing, medium absorbing and low absorbing solvents respectively.[24] Ethanol with tan $\partial > 0.941$ is more microwave absorbing than water with tan $\partial = 0.123$. The added ethanol in the synthesis of the gold seed solutions (AuNps) thus rapidly increases the temperature of the reaction.

FT-IR spectroscopy analysis of the AuNPs and Au@AgNPs performed on the NPs (**Figure 4**) shows that the overall characteristic of the gold particles differs from the bimetallic core shell NP, indicating that different capping agents were responsible for the stabilization of the particles. The Au@AgNPs revealed characteristics peaks at 1591 cm^{-1} (C=O asymmetric stretching in COO–) and 1396 cm^{-1} (C–OH stretching) and a broad absorption ban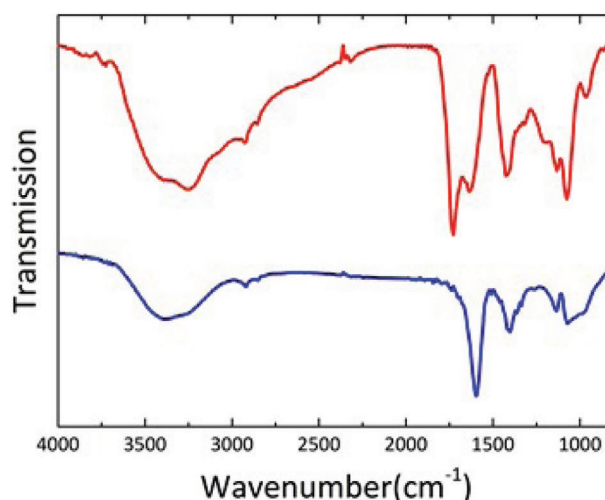d in the region between 3261 and 3388 cm^{-1} (hydrogen bonded OH stretching vibration of the carboxyl group) corresponding to functional groups that are characteristic for citrate. AuNPs exhibited multiple peaks at 1728 and 1624 cm^{-1}, 1421, 1205, 1126, 1068 cm^{-1}, indicating the presence of oxidized ester carbonyl and conjugated carbonyl groups. The peak at 1068 cm^{-1} corresponds to the C=O group of the primary hydroxyl stretching and a broad absorption band between 3244 and 3402 cm^{-1} corresponds to the hydroxyl group. This result indicates the presence of a "polyhydroxyl" structure,[25] which originates from sodium citrate and ascorbic acid on the gold surface. They both contribute to the strong capping effect. To further confirm the nature of capping agent on each of the AuNPs and Au@AgNPs further FT-IR investigations were performed and sodium citrate and ascorbic acid were used as references (Figure S8, Supporting Information). The peaks of the ascorbic acid spectrum are more pronounced in the AuNPs spectrum, while the sodium citrate peaks are in good agreement with the Au@AgNPs spectrum.

3. Core–Shell Nanoprism Synthesis

The strategy of introducing a stable organic bilayer barrier on the core surface was also explored for the synthesis of Au nanoprism cores to mediate the formation of Ag nanoprism. In this approach, the Au nanoprism synthesis was implemented by an utilization of combinations of HAuCl$_4$/ethanol/citrate/ascorbic acid and bis(p-sulfonatophenyl) phenylphosphine dihydrate dipotassium (BSPP) as triangular shape inducing agent. The formation of nanoprisms with truncated corners and spherical NPs was observed at a microwave power of 200 W for an irradiation time of 60 s (**Figure 5**). After this irradiation process, the as-synthesized NPs were used as seeds with combinations of aqueous solutions of silver acetate, sodium citrate, ascorbic acid and BSPP for the deposition of the silver shell at an increased MW power of 300 W for 60 s (**Figure 6**). Figure S9 (Supporting Information) provides a statistics of the particles present in the solutions.

ADVANCED
SCIENCE NEWS
www.advancedsciencenews.com

Particle
& Particle Systems Characterization
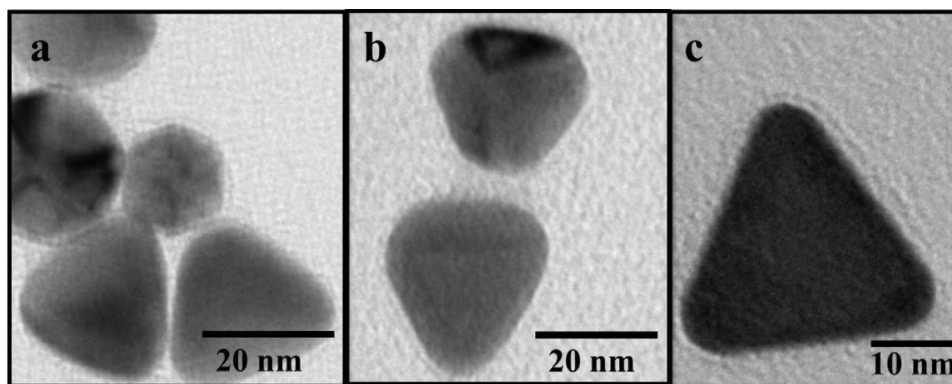www.particle-journal.com

Figure 5. TEM images of as-synthesized Au nanoprism at 200 W microwave power and 60 s irradiation time. a–c) Examples of gold nanoprisms synthesized by microwave irradiation.

In general, a good correlation arises between the shape of the core and the shell. The shell mainly resembles the corresponding core shape. However, in few cases, a prism Ag shell is formed around a spherical gold core and vice versa. These experiments nicely demonstrated the successful implementation of microwave-assisted synthesis processes and the tuning of a stable organic barrier layer which facilities the formation of well-defined core–shell NPs. However, the reason for the better stability of the citrate/ascorbic acid barrier layer remains unclear at this stage. A detailed investigation might provide insight into this issue, however, due to the fact that microwave synthesis of metallic particles does not allow to determine the actual reaction temperatures by means of the infrared sensor such investigations are difficult to establish. Selective heating processes
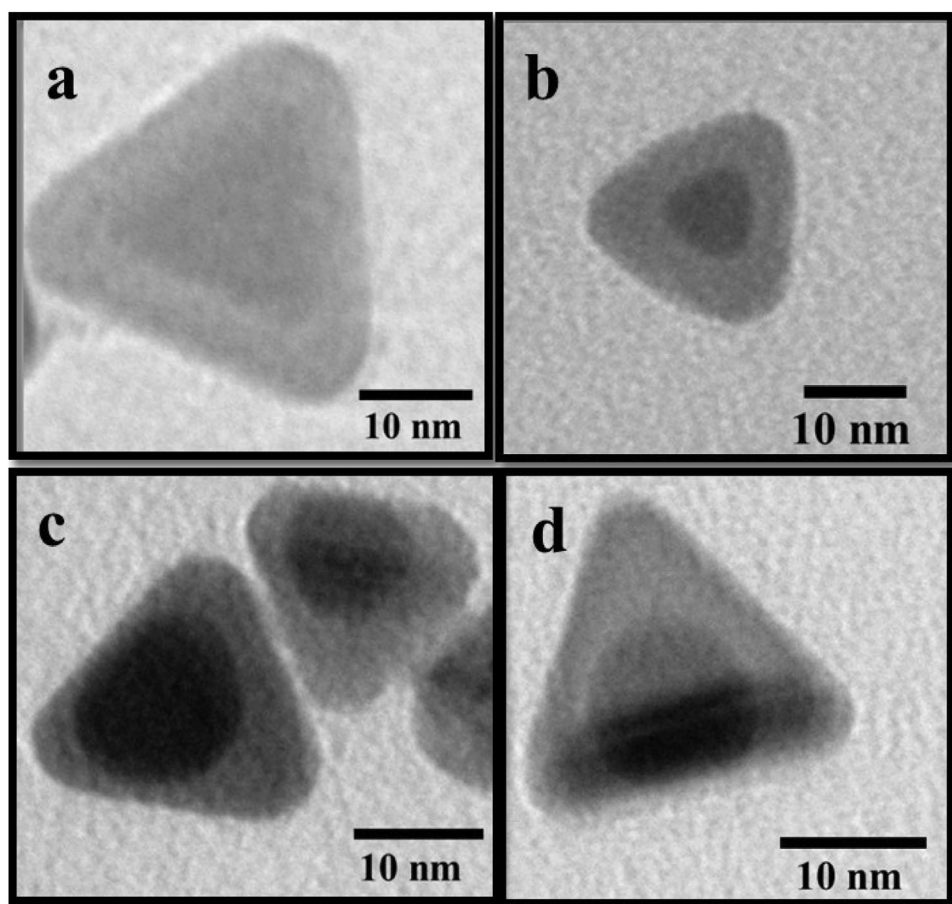

Figure 6. Representative TEM images of Au@Ag core–shell bimetallic nanoprisms synthesized at 300 W and 60 s irradiation time. a,b) Au prism cores surrounded by an Ag prism shell. c,d) Spherical Au core surrounded by an Ag shell.
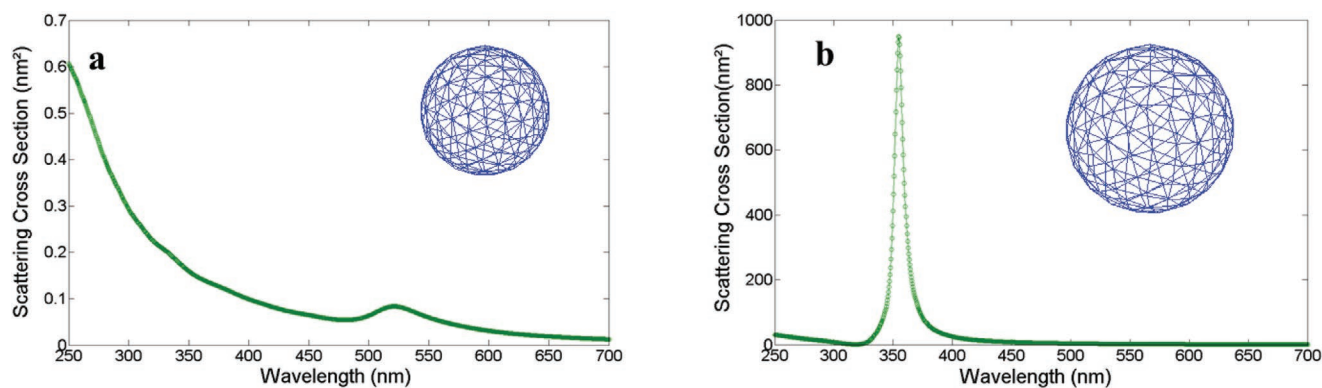
ADVANCED
SCIENCE NEWS
www.advancedsciencenews.com

Particle
& Particle Systems Characterization
www.particle-journal.com

Figure 7. Calculated spectrum of the scattering cross-section for a) 15 nm Au and b) 30 nm Ag.

of the metals might locally result in much higher temperatures as measured by this sensor. For this reason, these experimental conditions remain vastly unclear and prevent a final conclusion on the underlying mechanism at this stage.

The synthesized structures are very interesting for various applications in plasmonic engineering. In order to access the optical and plasmonic properties of such core–shell NPs simulations were performed by means of a boundary element method (BEM) approach. These simulations allow predicting the potential of the core–shell NPs in terms of the influence of the hybridization between the constituent metals and their plasmonic coupling.

These theoretical calculations of the optical characteristics of the NPs were performed with the Matlab based tool package "Metallic NP Boundary Element" (MNPBEM).[21] This toolbox offers a flexible approach for the plasmonic NP simulation. In order to identify suitable geometries to be established by means of the developed strategy to form core–shell NPs the scattering cross-sections of different geometries have been simulated based on the NP sizes and architectures found in the previous experiments.

First the scattering cross-section of an individual gold NP with a diameter of 15 nm was simulated. The obtained peak position for the LSPR peak at 522 nm (**Figure 7**a), is in good agreement with the absorbance maximum of respective UV–vis spectra of the particle solution which is found to be located at 524 nm (Figure 1b). The calculated λ_{max} of AgNP was at 354 nm (Figure 7b). It was additionally observed that the amplitude of the scattering in the AgNP is four orders of magnitude higher in comparison to that of the AuNP.

The calculation of the Au@Ag core–shell spherical NP revealed a strong change of the localized surface plasmon resonance and additional peaks arised due to the influence of plasmon-plasmon coupling effect between the core and the shell NPs. The combined and coupled resonances of the Au core and the oscillating modes of the Ag shell were observed by the appearance of multiple LSPR peaks in the spectra of the calculated scattering cross-section as shown in **Figure 8**a. Spectral resonance peaks are observed at 320, 334, 359, 482, and 522 nm, respectively. The peaks at 320, 334, and 359 nm correspond to the resonance of the Ag shell, while the peaks at 430 and 476 nm reflect the expected plasmon–plasmon coupling effect. The peak at 520 nm matches the resonance of the Au core. The diameters of the core and shell were set to 15

and 30 nm, respectively, according to the dimensions which were found in the synthesized NP systems by TEM investigations. In addition, the highest intensity coincides with that of the Ag shell. This trend is in agreement with the UV–vis spectrum shown in Figure 2d. Also in these experimental data the AgNP resonance peak dominates the spectrum. Due to ensemble averaging effects originating from the integration of a large number of Au@AgNPs which slightly differ in sizes and geometries, the characteristic peaks found in the simulations of an individual Au@AgNPs with distinct geometry cannot be resolved in the experimental UV–vis spectrum.

The optical characteristics of the NPs have been reported to depend on the shape of the NPs, thus, the LSPRs can be tuned by changing the morphology of the NPs.[25] For comparison, the scattering cross-section of a single Au NP with a diameter of 14.5 nm and a Ag nanoprism of 30 nm was simulated and the localized plasmon resonance frequencies of individual Au and Ag nanoprisms were identified at 535 and 390 nm, respectively (Figure S10, see the Supporting Information for calculated spectra). The optical tunability of core–shell NPs was explored by simulating the LSPRs of Au@Ag core–shell NPs. The case of a spherical 15 nm Au core embedded in a 30 nm Ag nanoprism shell, and another case of 14.5 nm Au nanoprism core in a 30 nm Ag nanoprism shell were simulated. In the former case (Figure 8a), multiple surface plasmon resonances can be seen at 320, 333, 355, 427, 488, and 520 nm. The additional peaks are ascribed to plasmon–plasmon coupling effects between the core and shell, which are observed at 427 and 488 nm. Similar multiple LSPR peaks were also seen for the particle architecture depicted in Figure 8c at 320, 334, 354, 431, 478, and 525 nm. Here, the resonances from the plasmon–plasmon coupling effects are observed at shifted wavelengths of 431 and 478 nm. This blue shift of more than the normal trend of ±3 nm at 488 nm (Figure 8b) to 478 nm (Figure 8c) could be attributed to the change of the aspect ratio of the core. In addition, the core–shell nanoprism–nanoprism entity in comparison to the sphere-sphere entity presents a higher scattering cross-section volume effect at the resonance peaks. This is due to the edges of the anisotropic structure.

The obtained results strongly suggest that the synthesized NP systems are highly attractive for plasmonic applications. Further experiments will be devoted to optimize the core–shell NP architectures and to study defined nanostructures formed by multiple core–shell assemblies.

**ADVANCED
SCIENCE NEWS**

www.advancedsciencenews.com

Particle
& Particle Systems Characterization
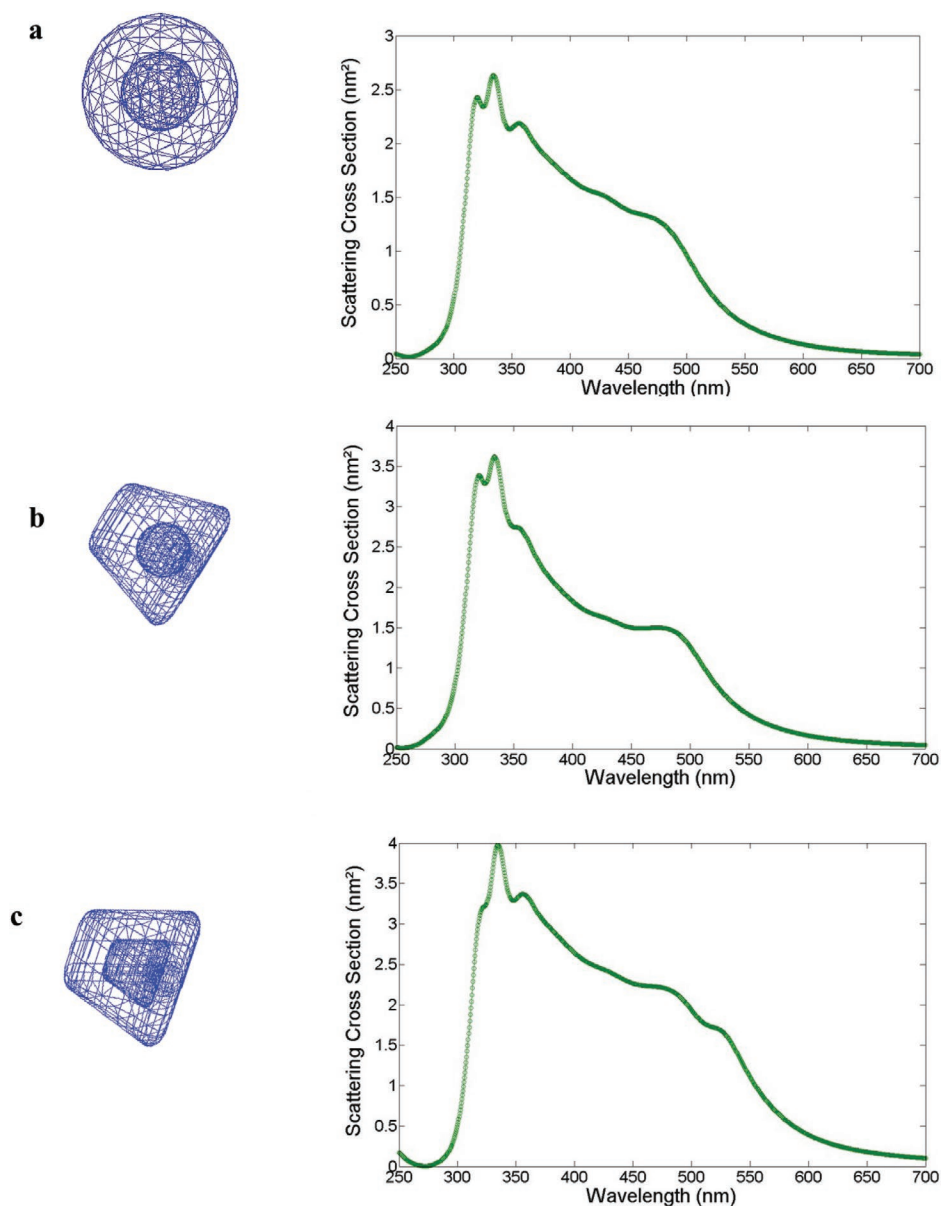
www.particle-journal.com

Figure 8. Calculated spectra of the scattering cross-section for a) spherical core–spherical shell Au@Ag NP b) spherical core–prism shell Au@Ag NP and c) Au@Ag nanoprism.

4. Conclusion

To efficiently tune the properties of bimetallic NP, a fast and simple method to synthesize core–shell NPs with a well-defined layer boundary has been established. A capping agent with a high stability is required for the core to protect the boundaries and also to provide an organic layer for the shell material attachment. In addition, it was found that when only citrate stabilized gold NPs were used as core a bimetallic alloy composite NP was formed rather than a core–shell structure. This is presumably due to the fact that the kinetic stabilization of the organic layer is impaired at high temperatures. In the case of the core–shell NPs, where ascorbic acid stabilized gold seeds were used as core, a well-defined boundary is attributed to the binding affinity of the polyhydroxyl structure in ascorbic acid for silver and, hence, initiates the formation of silver attachment at the core surface.

With this method core–shell bimetallic NPs with different geometries and structures can be synthesized in a fast as well as efficient microwave initiated synthesis strategy. Further variation of the concentrations of the metal precursor solution and the synthesis parameters can also be used to further tune the geometry of the particles, e.g., varying the shell thickness etc. The geometries and the shape of the core and the shell are important parameters to tune the plasmonic properties of the NPs. Applications of the core–shell NPs and defined arrangements of individual core–shell NPs will be subject of further studies and their potential for plasmonic applications will be further investigated.

5. Experimental Section

A typical experiment to synthesize gold NPs by microwave synthesis involves the collective mixing of $HAuCl_4$ solution (0.5 mL, 0.6×10^{-3} M), ethanol (1 mL), demineralized water (1.5 mL), sodium citrate (0.5 mL, 0.3×10^{-3} M), and ascorbic acid solution (0.5 mL, 0.6×10^{-3} M) in a 5 mL microwave vial at ambient temperature. A magnetic stirring bar is added and the microwave vial is capped with a Teflon septum. After microwave processing (Biotage Initiator), a characteristic color change from colorless to pink indicated the formation of gold NPs (seeds). The individually optimized microwave process parameters for the different NP architectures are listed in the main text.

1 mL as-synthesized gold NP colloid solution (seed) was further co-mixed with Ag acetate (0.5 mL, 0.6×10^{-3} M), ascorbic acid (0.5 mL, 0.6×10^{-3} M), demineralized water (1 mL) and sodium citrate (0.5 mL, 0.3×10^{-3} M) in a 5 mL microwave vial. A characteristic color change of the gold seed solution from pink to purple was observed, when silver acetate and ascorbic acid were added. Afterward, the vial was capped and subjected to 300 W microwave irradiation for 60 s. A color change from purple to a dark yellow was observed. TEM investigations were performed on a Tecnai G^2 20 (FEI). 15 mL of the NP solutions were blotted onto carbon coated TEM grids. FT-IR investigations were performed on a Tensor 27 (Bruker) operated in brewster-angle configuration.

Supporting Information

Supporting Information is available from the Wiley Online Library or from the author.

Conflict of Interest

The authors declare no conflict of interest.

[1] A. Knauer, A. Eisenhardt, S. Krischok, J. M. Koehler, *Nanoscale* **2014**, *6*, 5230.

[2] S. Kundu, K. Wang, H. Liang, *J. Phys. Chem. C* **2009**, *113*, 134.

[3] a) Y. X. Zhang, H. L. Ding, Y. Y. Liu, S. S. Pan, Y. Y. Luo, G. H. Li, *J. Mater. Chem.* **2012**, *22*, 10779; b) J. F. Li, Y. J. Zhang, S. Y. Ding, R. Panneerselvam, Z. Q. Tian, *Chem. Rev.* **2017**, *117*, 5002.

[4] X. Ding, P. Y. Yuan, N. Y. Gao, H. Zhu, Y. Y. Yang, Q. H. Xu, *Nanomedicine* **2017**, *13*, 297.

[5] M. Banerjee, S. Sharma, A. Chattopadhyay, S. S. Ghosh, *Nanoscale* **2011**, *3*, 5120.

[6] Y. W. Cao, R. Jin, C. A. Mirkin, *J. Am. Chem. Soc.* **2001**, *123*, 7961.

[7] L. H. Lu, H. S. Wang, Y. H. Zhou, S. Q. Xi, H. J. Zhang, H. B. W. Jiawen, B. Zhao, *Chem. Commun.* **2002**, 144.

[8] L. Lu, G. Burkey, I. Halaciuga, D. V. Goia, *J. Colloid Interface Sci.* **2013**, *392*, 90.

[9] a) M. A. Uppal, M. B. Ewing, I. P. Parkin, *Eur. J. Inorg. Chem.* **2011**, *2011*, 4534; b) R. Arenal, L. Henrard, L. Roiban, O. Ersen, J. Burgin, M. Treguer-Delapierre, *J. Phys. Chem. C* **2014**, *118*, 25643.

[10] L. P. Yang, W. J. Yan, H. X. Wang, H. Zhuang, J. H. Zhang, *RSC Adv.* **2017**, *7*, 11355.

[11] a) A. K. Samal, L. Polavarapu, S. Rodal-Cedeira, L. M. Liz-Marzan, J. Perez-Juste, I. Pastoriza-Santos, *Langmuir* **2013**, *29*, 15076; b) L. W. Dai, L. P. Song, Y. J. Huang, L. Zhang, X. F. Lu, J. W. Zhang, T. Chen, *Langmuir* **2017**, *33*, 5378.

[12] a) C. M. Gonzalez, Y. Liu, J. C. Scaiano, *J. Phys. Chem.* **2009**, *113*, 11861; b) H. X. Xu, B. W. Zeiger, K. S. Suslick, *Chem. Soc. Rev.* **2013**, *42*, 2555.

[13] S. K. Seol, D. Kim, S. Jung, Y. Hwu, *Mater. Chem. Phys.* **2011**, *131*, 331.

[14] a) M. E. El-Naggar, T. I. Shaheen, M. M. G. Fouda, A. A. Hebeish, *Carbohydr. Polym.* **2016**, *136*, 1128; b) D. V. Pryaznhikov, O. O. Efanova, M. S. Kiseleva, I. V. Kubrakova, *Nanotechnol. Russ.* **2017**, *12*, 199.

[15] a) I. Bilecka, M. Niederberger, *Nanoscale* **2010**, *2*, 1358; b) M. Baghbanzadeh, L. Carbone, P. D. Cozzoli, C. O. Kappe, *Angew. Chem., Int. Ed.* **2011**, *50*, 11312.

[16] M. Tsuji, N. Miyamae, S. Lim, K. Kimura, X. Zhang, S. Hikino, M. Nishio, *Cryst. Growth Des.* **2006**, *6*, 1801.

[17] J. C. Hernandez-Garrido, M. S. Moreno, C. Ducati, L. A. Perez, P. A. Midgley, E. A. Coronado, *Nanoscale* **2014**, *6*, 12696.

[18] J. Polte, *CrystEngComm* **2015**, *17*, 6809.

[19] M. Tsuji, M. Hashimoto, Y. Nishizawa, M. Kubokawa, T. Tsuji, *Chem. - Eur. J.* **2005**, *11*, 440.

[20] J. A. Gerbec, D. Magana, A. Washington, G. F. Strouse, *J. Am. Chem. Soc.* **2005**, *127*, 15791.

[21] H. J. You, J. X. Fang, *Nano Today* **2016**, *11*, 145.

[22] S. Pinero, S. Camero, S. Blanco, *J. Phys.: Conf. Ser.* **2017**, *786*, 012020.

[23] C. Xue, J. E. Millstone, S. Y. Li, C. A. Mirkin, *Angew. Chem., Int. Ed.* **2007**, *46*, 8436.

[24] D. Dallinger, C. O. Kappe, *Chem. Rev.* **2007**, *107*, 2563.

[25] P. K. Jain, K. S. Lee, I. H. El-Sayed, M. A. El-Sayed, *J. Phys. Chem. B* **2006**, *110*, 7238.